Computers and Geotechnics 37 (2010) 125–131

Contents lists available at ScienceDirect

Computers and Geotechnics

journal homepage: www.elsevier.com/locate/compgeo

Evaluating the performance of an explicit dynamic relaxation technique in analyzing non-linear geotechnical engineering problems

Hoang K. Dang, Mohamed A. Meguid *

Department of Civil Engineering and Applied Mechanics, McGill University, 817 Sherbrooke Street West, Montreal, Quebec, Canada H3A 2K6

ARTICLE INFO

Article history:
Received 13 February 2009
Received in revised form 15 June 2009
Accepted 7 August 2009
Available online 6 September 2009

Keywords:
Numerical modeling
Dynamic relaxation
Bearing capacity
Geotechnical engineering

ABSTRACT

Explicit dynamic relaxation is an efficient tool that has been used to solve problems involving highly non-linear differential equations. The key feature of this method is the ability to use explicit dynamic algorithms in solving static problems. Few attempts have been made to date to apply this technique in conventional geotechnical engineering. In this study, an algorithm that incorporates the application of a stiffness dependent time step scheme is proposed. The algorithm has been successfully used to solve 2D and 3D non-linear geotechnical engineering problems. To calibrate the developed algorithm, numerical simulations have been conducted for a strip and square footings supported by Mohr–Coulomb material. Performance of four different types of brick elements used in collapse load calculation is examined in terms of convergence speed and accuracy. In addition, the role of employing adaptive time steps in reducing the number of iterations needed for convergence is also evaluated.

1. Introduction

With the continuous increase in computing power, more complex engineering problems are being considered in computational mechanics. However, the cost of solution and storage requirement increases dramatically for large scale three-dimensional (3D) problems. This has lead to an increased interest in parallel computing techniques making direct solvers (in static analysis) and implicit time integration methods (in dynamic analysis) less competitive compared to the iterative solvers and explicit or mixed time integration procedures. In addition, the development of combined numerical methods (such as finite/discrete element) necessitates the use of consistent integration schemes for both finite and discrete element domains. Since explicit methods are commonly used in discrete element analysis, they are therefore needed for the analysis of the finite element domain.

Over the past few decades, different static problems have been successfully analyzed using the dynamic relaxation (DR) methods (e.g. Felippa [1] and Underwood [2]). In DR methods, the response of a given structure is damped until it reaches a steady state. The convergence speed of the explicit DR methods is generally proportional to the ratio of the highest to the lowest eigenvalues of the stiffness matrix [3]. Although the performances of implicit versus explicit methods is generally hard to judge, for a 3D homogenous finite element mesh, this ratio is proportional to N and $N^{2/3}$ for implicit and explicit methods, respectively [3]. Furthermore, Xie [4] reported that the unconditional stability of implicit methods in linear analysis is no longer valid in non-linear analysis. The reliability of the DR solutions is usually ensured by using integration parameters that are adaptively changing throughout the analysis to account for the non-linear effects. Although a small time step is required to ensure numerical stability, the computational cost per time step is generally low.

Oakley and Knight [5] developed an adaptive DR for non-linear hyperelastic structures. An adaptive time step and mass proportional damping coefficient are calculated based on global tangent stiffness. Sauvé and Metzger [6] applied the DR to solve geometrically non-linear structural engineering problems with creep material. A modification to the mass proportional damping is developed by Metzger [7] to avoid the deleterious effects of sudden changes in the damping coefficient. Shoukry et al. [8] used the DR with constant time step to study the response of the pavement under thermal loading.

Given the numerical efficiency of the DR methods, attempts have been made to solve geotechnical engineering problems involving highly non-linear material models. Siddiquee et al. [9] proposed an explicit dynamic relaxation technique to simulate the bearing capacity of a strip footing on sand under plane strain condition. The time step was kept constant and several techniques were proposed to maintain the stability of the integration (e.g. load control, arc length control and displacement control). However, the above technique requires a careful user control to maintain the stability of the analysis. Tanaka [10] applied the same techniques to study the response of a single element under plane

* Corresponding author. Tel.: +1 514 398 1537; fax: +1 514 398 7361.
E-mail addresses: kien.dang@mail.mcgill.ca (H.K. Dang), mohamed.meguid@mcgill.ca (M.A. Meguid).

0266-352X/$ - see front matter © 2009 Elsevier Ltd. All rights reserved.
doi:10.1016/j.compgeo.2009.08.004

strain condition. The simulations were carried out assuming plane strain and using a fine mesh of linear quadrilateral element.

As the stress state violates the failure criteria, the element stiffness can no longer be calculated purely based on elastic formulation. The stiffness of the element often decreases significantly when plasticity occurs. Since the time step depends on the element stiffness, the time step can be adjusted as plasticity develops resulting in accelerated steady state.

In this study, a modified framework of dynamic relaxation applicable to plastic material is proposed. The time step is calculated based on the element consistent tangent stiffness that depends on the constitutive model. The algorithm is validated by simulating the bearing capacity of a strip and square footings. The effect of the adaptive time step calculated based on element consistent tangent stiffness is also evaluated. In addition, the performance of several solid elements commonly used in 3D analysis is examined.

The developed algorithm and the finite element library were implemented as a finite element package into the Discrete Element Open Source code YADE [11] using C++ programming as part of the ongoing development of a generalized discrete-finite element framework for geotechnical applications.

2. Governing equations and force description

The developed algorithm was based on the adaptive dynamic relaxation (ADR) method proposed by Oakley and Knight [5] with the addition of a simple plasticity model. The spatial discretization of a damped structural system can be written as

$$Kx + C\dot{x} + M\ddot{x} = P \tag{1}$$

where K, C and M are the stiffness, damping and the mass matrix, respectively, x represents the displacement vector and P is the external force vector. The internal force vector F can be assembled on an element by element basis.

The solution of Eq. (1) was obtained using an explicit time integration technique. In this study the central-difference scheme was adopted as it has been proven to be computationally efficient [4]. To avoid the need for the assembly and factorization of the global matrices, a mass proportional damping (cM) together with a diagonal mass matrix (M) obtained using mass lumping were employed. The lumped mass matrix can also increase the numerical stability of the explicit time integrator [12]. The errors introduced by the lumped masses are compensated for by the central difference operator [13]. Eq. (1) can therefore be written as

$$Kx + cM\dot{x} + M\ddot{x} = P \tag{2}$$

where c is the damping coefficient for mass proportional damping.

3. Time step equation

In the central difference method, the velocities are defined at the mid point of the time step, and the approximation for the temporal derivatives is given as:

$$\dot{x}^{n+1/2} = \frac{1}{\Delta t}(x^{n+1} - x^n) \tag{3}$$

$$\ddot{x}^n = \frac{1}{\Delta t}(\dot{x}^{n+1} - \dot{x}^n) \tag{4}$$

where Δt is the fixed time step increment. There are generally two options to derive an incremental relationship: (1) assuming constant acceleration over Δt; (2) assuming constant velocity over Δt. In this study, the latter assumption was adopted and the velocity was taken as the average value over Δt:

$$\dot{x}^n = \frac{1}{2}(\dot{x}^{n+1/2} + \dot{x}^{n-1/2}) \tag{5}$$

Substituting Eqs. (3)–(5) into Eq. (2), the expressions for advancing the velocity and displacement vectors, respectively, can be written as:

$$\dot{x}^{n+1/2} = \frac{2 - \Delta tc}{2 + \Delta tc}(\dot{x}^{n-1/2}) + \frac{2\Delta t}{2 + \Delta tc}M^{-1}(P^n - F^n) \tag{6}$$

$$x^{n+1} = x^n + \Delta t\dot{x}^{n+1/2} \tag{7}$$

where F^n and P^n are the internal and external force vectors, respectively, at time step increment n. The inverse matrix of M is trivial since M is diagonal. For the first time step, the velocity can be calculated as

$$\dot{x}^{1/2} = -\frac{\Delta t}{2}M^{-1}(P^0 - F^0) + \frac{1}{2}(2 - \Delta tc)\dot{x}^0 \tag{8}$$

Since the objective of the ADR is to determine the steady state solution of the pseudo-transient response, it is important to determine the stability condition (or convergence criterion) when the system is static. The stability condition is determined considering the relative errors in the body forces from one step to the next

$$e = \frac{\|F^n - F^{n-1}\|}{\|F^n\|} \leqslant tol \tag{9}$$

4. Stability of time steps

For the stability of the central difference integrator, the time step must be smaller than a limit derived based on the well known Courant–Friedrichs–Lewy condition.

$$\Delta t \leqslant \frac{2}{\sqrt{\lambda_m}} \tag{10}$$

where λ_m is the maximum eigenvalue. An upper bound to the maximum eigenvalue can be obtained from Gerchgorin's theorem as:

$$\lambda_m \leqslant \max \sum_{j=1}^{n} \frac{|K_{ij}|}{M_{ii}} \tag{11}$$

where K_{ij} is an element of the element consistent tangent stiffness matrix. K_{ij} is derived from the return mapping algorithm described in the constitutive modeling section. It should be noted that both the mass (either real or virtual) and time step size are not independent. Adjusting the mass can lead to inaccurate results particularly when time dependent loading is applied. Thus the mass has been fixed in the proposed algorithm and the time step has been adjusted based on the changes in the element consistent tangent stiffness.

5. Optimal convergence

Rapid convergence is usually obtained when the ratio of the maximum to minimum eigenvalues is as small as possible. As shown by Oakley and Knight [5], the optimal convergence condition is reached if

$$c \leqslant 2\sqrt{\lambda_0} \tag{12}$$

where λ_0 is the minimum eigenvalues. To estimate the minimum eigenvalue, the mass-stiffness Rayleigh quotient can be used such that

$$\lambda_0 \cong \frac{(\dot{x}^{n-1/2})^T S^n \dot{x}^{n-1/2}}{(\dot{x}^{n-1/2})^T M \dot{x}^{n-1/2}} \tag{13}$$

where S is the lumped stiffness matrix for linear problems. For nonlinear problem, S^n is determined as follows

$$S^n \cong \frac{F^n - F^{n-1}}{\Delta t \dot{x}^{n-1/2}} \tag{14}$$

No additional parameters are required as the algorithm automatically adjusts the optimal damping coefficient and the time step based on the changes in the element consistent tangent stiffness.

6. Constitutive model

Plasticity models in geomechanics can be integrated using either explicit integration (forward Euler) or implicit integration (backward Euler). The first is simple to be implemented and generally is employed for element-base analysis. However, if the material is highly non-linear, much iteration may be needed to return the stress state to the failure surface. Moreover, as the stress state violates the failure criteria, the element stiffness can no longer be calculated purely by elastic formulation. Since the element stiffness decreases significantly when plasticity develops and the time step depends on the element stiffness (see Eq. (10)), the time step can therefore be increased resulting in that the steady state condition can be achieved faster. The closest point projection method (CPPM) with consistent elastoplastic modulus was utilized at the Gauss points to calculate the element tangent stiffness. The procedure to derive the consistent tangent stiffness is described below.

In CPPM, the increments of plastic strain are calculated at the end of each iteration step. Similarly, the yield condition is enforced at the end of the step (Simo and Hughes [14]). The integration scheme is written in incremental form as

$$d\varepsilon^p = d(\Delta\lambda)q + \Delta\lambda dq \tag{15}$$

$$d\sigma = D^e(d\varepsilon - d\varepsilon^p) \tag{16}$$

$$df = a^T d\sigma = 0 \tag{17}$$

where $d\varepsilon^p$, $d\sigma$ and $d\varepsilon$ is the incremental plastic strain, incremental stress and incremental total strain, respectively, $\Delta\lambda$ is the plastic multiplier.

$$a = \left(\frac{\partial f}{\partial \sigma}\right) \tag{18}$$

where f is the yield function.

$$dq = \left(\frac{\partial q}{\partial \sigma}\right) d\sigma \tag{19}$$

where q is the derivative of the plastic flow potential function g with respect to stress.

Plastic multiplier can be updated consequently at iteration $(k+1)$th based on iteration kth

$$\Delta\lambda^{k+1} = \Delta\lambda^k + \delta\lambda^k \tag{20}$$

where $\delta\lambda^k$ is the increment in $\Delta\lambda$ at k iteration. $\delta\lambda^k$ is calculated as follows

$$\delta\lambda^k = \frac{f^k - a^{(k)T} R^{(k)} r^{(k)}}{a^{(k)T} R^{(k)} q^{(k)}} \tag{21}$$

where

$$R^k = \left[I + \Delta\lambda^k D^e \left(\frac{\partial q}{\partial \sigma}\right)^k \right]^{-1} D^e \tag{22}$$

and

$$r^k = -\varepsilon^p + \varepsilon^p_{accumulated} + \Delta\lambda q \tag{23}$$

where $\varepsilon^p_{accumulated}$ is the total plastic strain accumulated at the previous load step.

Substituting Eq. (15) into (16) with condition given by Eq. (17) and solving for $d(\Delta\lambda)$ gives

$$d(\Delta\lambda) = \frac{a^T R d\varepsilon}{a^T R dq} \tag{24}$$

Substituting into Eq. (16) gives

$$d\sigma = D^c d\varepsilon \tag{25}$$

where D^c is the consistent elastoplastic modulus calculated as

$$D^c = R - \frac{Rqa^T R}{a^T Rq} \tag{26}$$

To approximate the consistent stiffness of the element, the B matrix derived from the shape function of the element was employed. The element consistent tangent stiffness K^c_e then can be determined as:

$$K^c_e = \int_{\Omega_e} B^T D^C B d\Omega \tag{27}$$

The flow chart used in the development of the proposed algorithm is shown in Fig. 1.

7. Calibration of the proposed algorithm

The proposed algorithm was used to simulate the bearing capacity of a strip and square footings in weightless soil. The footings were assumed to be rigid enough to create uniform pressure on the supporting soil. The Mohr Coulomb (MC) failure criterion with non associated flow rule was utilized in both cases. Local rounding at the corners of the MC failure surface in the principal stress space was used as described by Smith and Griffiths [15]. The material properties are summarized in Table 1. The calculated load displacement behaviour for the two investigated cases was established and compared with the conventional static analysis using the same mesh and material properties.

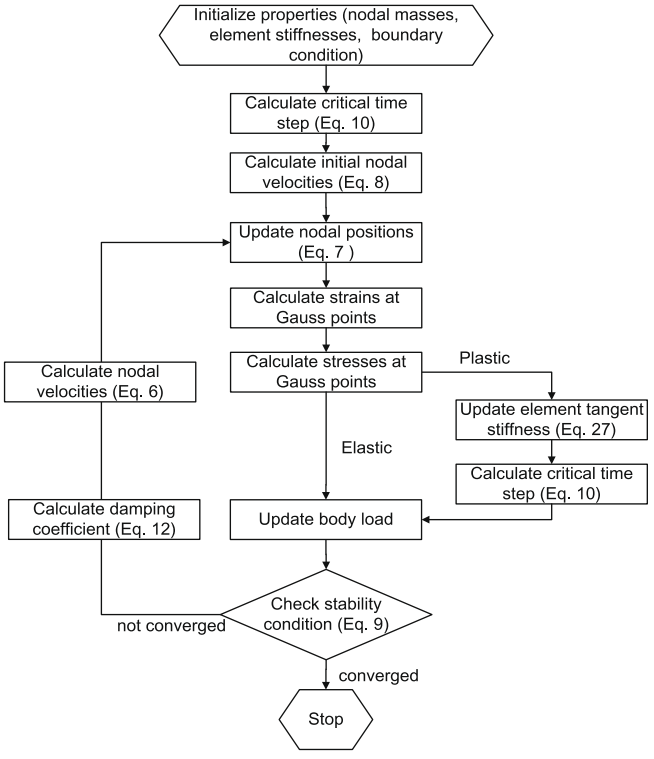

Fig. 1. Flow chart for the adaptive explicit dynamic relaxation.

Table 1
Material properties.

Cases	Cohesion (Pa)	Friction angle (°)	Dilation angle (°)	Poisson's ratio	Young's modulus (Pa)	Unit weight (kN/m^3)
Strip footing drained condition	35	20	0	0.3	1×10^5	0
Square footing drained condition	35	20	0	0.3	1×10^5	0
Square footing undrained condition	100	0	0	0.49	1×10^5	0
Square footing drained condition (used in the numerical example)	0.1	30	30	0.3	1×10^6	18

Theoretically, the bearing capacity can be calculated as

$$q_{ult} = cN_c \tag{28}$$

where N_c is the bearing capacity factor expressed as (Prandtl [16])

$$N_c = (N_q - 1)\cot\phi \tag{29}$$

where

$$N_q = \tan^2(45 + \phi/2)e^{\pi\tan\phi} \tag{30}$$

For the drained case $N_c = 14.83$ and $q_{ult} = 520$ kPa; for the undrained case $N_c = 5.14$ and $q_{ult} = 514$ kPa.

7.1. Strip footing

The analyzed footing is 4 m wide and supported by Mohr Coulomb drained material. Drained condition was carried out using plane strain analysis. Considering the symmetry of the problem, only one half of the footing was analyzed. Quadratic quadrilateral elements with reduced integration (4 Gauss points) were employed in the simulation. The problem geometry and the finite element mesh are shown in Fig. 2. In order to capture the failure load, a uniform pressure of 200 kPa was first applied at the initial step. After the stability condition (expressed by Eq. (9)) was reached, the load was then increased to the next step. A tolerance value of 1e−6 was adapted in the present analysis. Seven load increments of: 200 kPa, 300 kPa, 350 kPa, 400 kPa, 450 kPa, 480 kPa and 500 kPa were applied to approach the expected failure load. The load was subsequently increased (1 kPa increments) up to failure which is characterized by the numerical instability of the system.

In conventional implicit analysis, the applied load must be divided into several increments to reach convergence and maintain stability. If the stress state is far from the yield surface, the correct stress state cannot be easily determined. To demonstrate the robustness of the algorithm in modeling highly non-linear material, the total load was applied in one single step and the displacement results were compared with the previous multi-step analysis.

As shown in Fig. 3, the results of the dynamic relaxation analyses are in good agreement with those obtained using the conventional static analysis. Both of the simulations captured the theoretical Prandtl failure load (514 kPa). It can also be seen that the single step loading has successfully produced the same response.

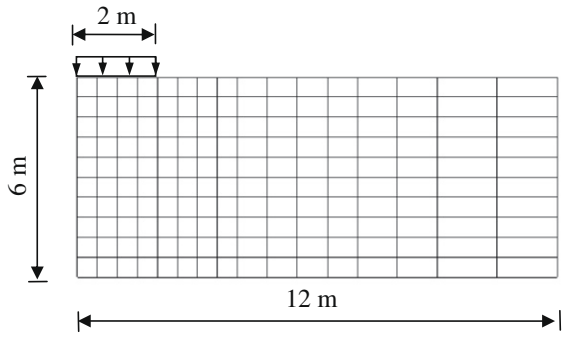

Fig. 2. Finite element mesh used in the strip footing analysis.

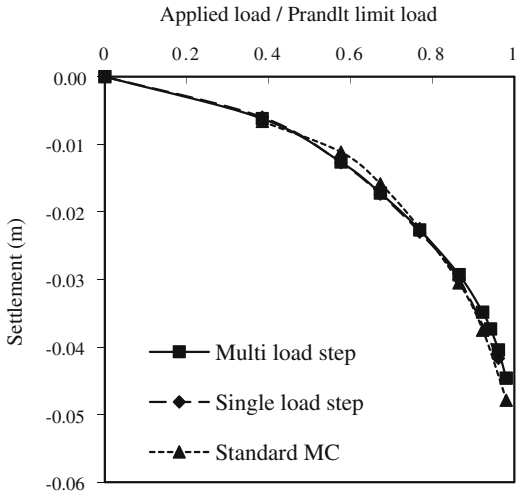

Fig. 3. Load–displacement relationships for the strip footing under drained condition.

7.2. Square footing

The bearing capacity of a square footing 4 m × 4 m was analyzed under both drained and undrained conditions. A schematic of the problem geometry and the 3D finite element mesh (1728 elements) are illustrated in Fig. 4. Due to the symmetry, only 1/4 of the footing was modeled. The mesh in the vicinity of the footing was refined to capture the rapid changes in displacement gradients. Smooth rigid side boundaries and a rough rigid base boundary were used in the analysis.

The performance of four different finite elements was also investigated in terms of speed and accuracy. The examined element types are listed below:

1. Reduced integration twenty-node quadratic brick elements (20N8I).
2. Mixed integration rule eight-node quadratic brick elements (8NS8I) (Simo and Rifai [17]).
3. Reduced integration eight-node quadratic brick elements (8N1I).
4. Reduced integration eight-node quadratic brick elements with stiffness hourglass control (8NH1I) (Belytschko and Ong [18]).

The finite element meshes generated using the above elements were further refined to examine the effect of the element size on the calculated displacements. As shown in Fig. 5, the load displacement curves exhibited little difference in all of the examined cases. The failure loads captured by the different elements varied from 1.08 to 1.23 times of the Prandtl load. The calculated values are

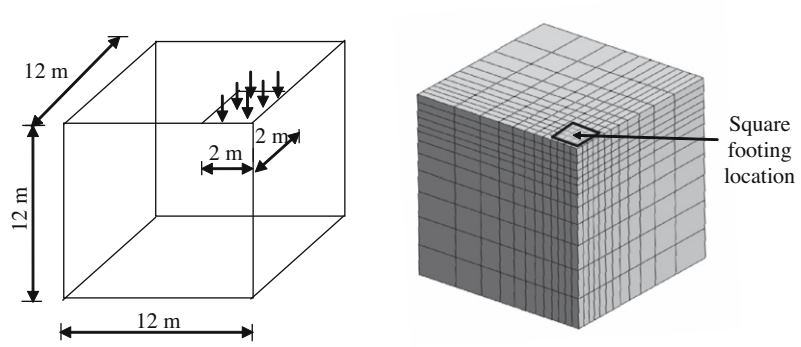

Fig. 4. Geometry and finite element mesh for the square footing.

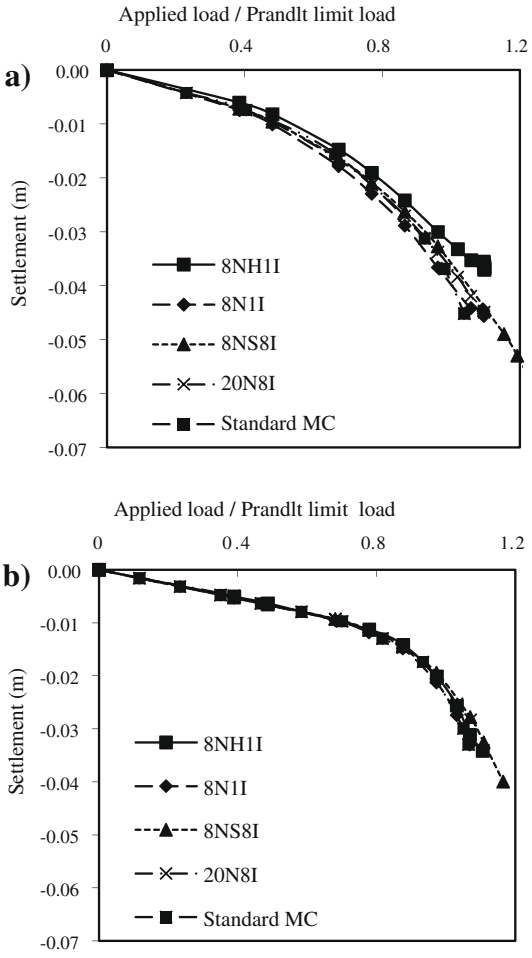

Fig. 5. Load–displacement relationships for the square footing: (a) drained condition and (b) undrained condition.

consistent with those reported by Salgado et al. [19] for rectangular footings. It is worth noting that the captured failure loads and the load displacement behaviour of the 8NH1I elements varied depending on the value of the anti hourglass parameter.

It was also found that the 8N1I element (usually unstable element due to the deficient stiffness ranking) performed reasonably well using the proposed algorithm. Similarly for the undrained analysis where soil experienced constant volume deformation, no hourglass displacements were observed. This can be explained by the dominating shear failure of the supporting soils. The computational times for all examined cases are summarized in Table 2. It can be seen that the 20N8I required the most time among all examined elements, however, it provided an accurate failure load prediction. 8NH1I and 8N1I elements are the most economical in terms of analysis time meanwhile the accuracy is preserved. However, due to the formulation deficiency, the use of 8N8I is not recommended for collapse analysis. It is concluded that the 8NH1I has maintained the balance between the calculation speed and the accuracy and therefore is considered to be the best choice for the above type of analysis.

Table 2
Computation time (min).

Cases	20N8I	8NS8I	8NH1I	8N1I
Square footing drained condition	156	12	4	3
Square footing undrained condition	195	30	6	5

8. Effect of using adaptive time step scheme

The effect of the adaptive time step in 2D and 3D analyses is illustrated in Fig. 6. When the load applied was less than 45% of the failure load, no significant effect was observed. However, increasing the applied load to about 70% of the failure load resulted in an increase in the number of iterations needed for convergence in both the constant time step and adaptive time step schemes. However, the constant time step scheme required 1.4 times the number of iterations needed for the adaptive time step scheme. The ratio slightly decreased as the applied load approached failure and the difference between the two schemes decreased to about 1.2.

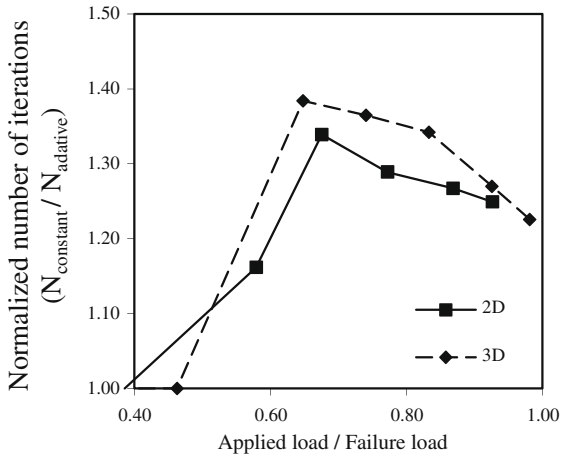

Fig. 6. Comparison between constant and adaptive time step schemes.

9. Numerical example

A square footing supported by Mohr Coulomb drained material is analyzed using the developed algorithm adopting the problem geometry shown in Fig. 4. The soil unit weight is assumed to be 18 kN/m^3 with friction angle of 30°. The material properties used in the analysis are provided in Table 1. The bearing capacity of the footing has also been calculated based on Terzaghi [20] bearing capacity theory:

$$q_{ult} = cN_c + qN_q + \frac{1}{2}\gamma BN_\gamma \tag{31}$$

where q is the overburden pressure; γ is the soil unit weight; B is the footing width; N_γ is derived by Michalowski [21] as follows:

$$N_\gamma = e^{0.66+5.11\tan\phi}\tan\phi \tag{32}$$

Thus for sand with friction angle of 30, a value of 771 kN/m^2 is obtained for the bearing capacity of the square footing.

The same mesh in the previous section was used with 8NH1I elements (see Fig. 4). An additional feature of the analysis is the activation of the soil unit weight and the initial stresses assigned at Gaussian stress points. The coordinates of each Gauss point are calculated using the isoparametric property of the element

$$y = \sum_{i=1}^{8} N_i y_i \tag{33}$$

where N is the shape function of the brick element and y is the vertical coordinate of the element nodes. Only the y coordinate is required in this case and the vertical stress σ_y is obtained after multiplication by the soil unit weight (Table 1). The normal effective stresses σ_x and σ_z are obtained by multiplying σ_y by the earth pressure coefficient at rest (K_0) calculated using (Jaky, [22]):

$$K_0 = 1 - \sin\phi \tag{34}$$

The analysis consists of two stages: Geostatic stage and failure load analysis. In the geostatic stage, the soil weight is activated and the equilibrium is first obtained. In the next stage, the same procedure used in Section 7 is employed to determine the failure load.

As shown in Fig. 7, the calculated failure load is found to be 862 kN/m^3, the ratio of the calculated value to the theoretical value (approximately 1.12) agrees well with that reported by Ming and Michalowski [23]. It is worth noting the analysis reported by Ming and Michalowski [23] employing the implicit methods required the use of a cohesion value of 3.6 kPa in order to maintain convergence whereas in the present study no such assumption was needed to achieve convergence.

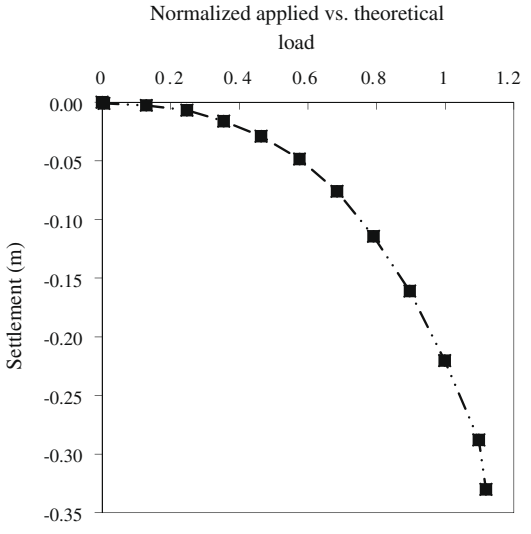

Fig. 7. Load–displacement relationships for a square footing on sand.

10. Summary and conclusions

An adaptive dynamic relaxation method applicable to geotechnical applications was developed and implemented in this study. The use of diagonal mass and damping matrices with central difference time integrator has proven to be an effective numerical approach for problems involving material nonlinearity. Adjusting the adaptive time step based on the changes in the element consistent tangent stiffness resulted in a decrease in the number of iterations needed for convergence by up to 40% compared to the constant time step schemes. In the proposed algorithm, the time step and damping values were automatically adjusted to achieve an optimal convergence while maintaining the stability of the system. The robustness and accuracy of the algorithm were demonstrated by analyzing the bearing capacity of strip and square footings.

The performance of four different brick elements was also evaluated. The accuracy of the eight-node brick element with stiffness hourglass control was found to be heavily dependent on the user experience. Finally, since the proposed finite element algorithm employs a explicit dynamic scheme that is commonly adopted in Discrete Element analysis, it in can be easily combined with a Discrete Element code in developing a hybrid Discrete-Finite element suitable for geotechnical engineering applications.

Acknowledgements

This research is supported by a research grant from the Natural Sciences and Engineering Research Council of Canada (NSERC). The financial support provided by McGill Engineering Doctoral Award (MEDA) to the first author is greatly appreciated.

References

[1] Felippa CA. Dynamic relaxation in quasi-Newton methods. In: Taylor C, Hinton E, Owen DRJ, Onate D editors. Numerical methods for nonlinear problems, Swansea; 1986. p. 27–38.
[2] Underwood PG. Dynamic relaxation: a review. In: Belytschko T, Hughes TJR editors. Computational methods for transient dynamic analysis, North Holland, Amsterdam; 1983 [chapter 5].
[3] Munjiza A. The combined finite-discrete element method. England: John Wiley & Sons Ltd.; 2004.
[4] Xie YM. An assessment of time integration schemes for non-linear dynamic equations. J Sound Vib 1996;192(1):321–31.
[5] Oakley DR, Knight NF. Adaptive dynamic relaxation algorithm for non-linear hyperelastic structures Part I. Formulation. Comput Method Appl Mech Eng 1995;126(1):67–89.
[6] Sauvé RG, Metzger DR. Advances in dynamic relaxation techniques for nonlinear finite element analysis. J Press Vessel Technol 1995;117:170–6.
[7] Metzger DR. Adaptive damping for dynamic relaxation problems with non-monotonic spectral response. Int J Numer Method Eng 2003;56:57–80.
[8] Shoukry SN, William GW, Riad MY, McBride KC. Dynamic relaxation: a technique for detailed thermo-elastic structural analysis of transportation structures. Int J Comput Method Eng Sci Mech 2006;7(4):303–11.
[9] Siddiquee MSA, Tanaka T, Tatsuoka F. Tracing the equilibrium path by dynamic relaxation in materially nonlinear problems. Int J Numer Anal Method Geomech 1995;19(11):749–67.
[10] Tanaka T. Viscoplasticity of geomaterials and finite element analysis. In: Soil stress strain behavior: measurement, modeling and analysis, geotechnical symposium in Rome, March; 2006. p. 769–78.
[11] Kozicki J, Donze FV. Applying an open-source software for numerical simulations using finite element or discrete modelling methods. Comput Method Appl Mech Eng 2008;197(49–50):4429–43.
[12] Belytschko T, Mullen R. Explicit integration of structural problems. In: Finite elements in nonlinear mechanics, TAPIR, Trondheim; 1978.
[13] Krieg R, Key S. Transient shell response by numerical time integration. Int J Numer Method Eng 1973;17:273–86.
[14] Simo JC, Hughes TJR. Computational inelasticity. New York: Springer; 1998.
[15] Smith IM, Griffiths DV. Programming the finite-element method. 4th ed. New York: Wiley; 2004.

[16] Prandtl L. Uber die Eindringungsfestigkeit (Härte) plastischer baustoffe und die festigkeit von Schneiden. Z angew Mathe Mech 1921;1(1):15–20.
[17] Simo JC, Rifai MS. A class of mixed assumed strain methods and the method of incompatible modes. Int J Numer Method Eng 1990;29:1595–638.
[18] Belytschko T, Ong S. Hourglass control in linear and nonlinear problems. Comput Method Appl Mech Eng 1984;43:251–76.
[19] Salgado R, Lyamin A, Sloan S, Yu HS. Two- and three-dimensional bearing capacity of footings in clay. Geotechnique 2004;54(5):297–306.
[20] Terzaghi K. Theoretical soil mechanics. New York: Wiley; 1943.
[21] Michalowski RL. An estimate of the influence of soil weight on bearing capacity using limit analysis. Soils Found 1997;37(4):57–64.
[22] Jaky J. Pressure in soils. 2nd ed. London: ICSMFE; 1948, vol. 1. p. 103–7.
[23] Ming Z, Michalowski RL. Shape factors for limit loads on square and rectangular footings. J Geotechn Geoenviron Eng 2005;131:223–31.